

## Membrane-Bound Dynamic Structure of an Arginine-Rich Cell-Penetrating Peptide, the Protein Transduction Domain of HIV TAT, from Solid-State NMR<sup>†</sup>

Yongchao Su,<sup>‡</sup> Alan J. Waring,<sup>§</sup> Piotr Ruchala,<sup>§</sup> and Mei Hong\*,<sup>‡</sup>

<sup>‡</sup>Department of Chemistry, Iowa State University, Ames, Iowa 50011, and <sup>§</sup>Department of Medicine, David Geffen School of Medicine, University of California at Los Angeles, Los Angeles, California 90095

Received April 26, 2010; Revised Manuscript Received June 12, 2010

**ABSTRACT:** The protein transduction domain of HIV-1 TAT, TAT(48–60), is an efficient cell-penetrating peptide (CPP) that diffuses across the lipid membranes of cells despite eight cationic Arg and Lys residues. To understand its mechanism of membrane translocation against the free energy barrier, we have conducted solid-state NMR experiments to determine the site-specific conformation, dynamics, and lipid interaction of the TAT peptide in anionic lipid bilayers. We found that TAT(48–60) is a highly dynamic and nearly random coil peptide in the lipid bilayer and inserts into the membrane–water interface near the glycerol backbone region. Arg–phosphate salt bridge interaction was revealed by short guanidinium–phosphate distances and restricted dynamics of the guanidinium. Together with the observation of strong peptide–water cross-peaks in <sup>1</sup>H spin diffusion spectra, these results indicate that TAT binding to the membrane–water interface is stabilized not only by electrostatic attraction to the anionic lipids but also by intermolecular hydrogen bonding with the lipid phosphates and water, which may take the role of intramolecular hydrogen bonds in canonical secondary structures. The random coil structure of TAT and another CPP, penetratin, suggests that the lack of amphipathic structure is essential for rapid translocation of these Arg-rich CPPs across the lipid membrane without causing permanent damages to the membrane integrity.

Cell-penetrating peptides (CPPs)<sup>1</sup> are highly cationic and Arg-rich peptides that are able to cross lipid membranes into cells both alone and in conjugation with large macromolecular cargos (1, 2). Therefore, CPPs are potentially important molecules for drug delivery and for studying macromolecular structures inside living cells (3). CPPs have been discovered from diverse origins such as the TAT protein of HIV-1 (4), penetratin from the *Drosophila antennapedia* homeodomain (5), and synthetic polyarginine peptides (6, 7). In contrast to antimicrobial peptides (AMPs), which are similarly Arg-rich sequences but which kill bacterial cells by disrupting their lipid membranes, CPPs appear to enter eukaryotic cells without causing long-lasting damage to the integrity of the cell membrane.

The physical basis for the membrane translocation of CPPs has been much debated and is still not well understood (8). It is well-known that the low-dielectric interior of cell membranes presents a high-energy barrier to the direct unassisted diffusion of charged ions and molecules. The free energies of transfer of amino acid residues from the aqueous to a nonpolar solvent have been measured experimentally and are highly positive for Arg

and Lys (9). It is thus puzzling how short peptides containing a high density of Arg residues are able to cross the membrane. Two models, an inverse micelle model (10) and an electroporation model (11), had been proposed to account for membrane translocation of CPPs, but neither was supported by recent solid-state NMR studies of penetratin. Specifically, <sup>31</sup>P NMR line shapes indicated the absence of isotropic entities in the membrane, thus ruling out the inverse micelle model (12). Paramagnetic relaxation enhancement experiments using Mn<sup>2+</sup> ions bound to the outer surface of lipid bilayers versus both surfaces indicated that penetratin was distributed equally in the two leaflets of the membrane even at low peptide concentrations (12). This finding contradicted the electroporation model, which posits that asymmetric association of CPPs with the outer leaflet of the membrane causes an electric field that alters the lateral and curvature stress of the membrane, eventually causing electroporation-like perforation of the membrane (11). Instead, site-specific distances between penetratin and the lipid headgroups indicated tight guanidinium–phosphate associations (13), suggesting that ion pair interaction between the Arg residues and the anionic lipid headgroups may play a significant role in the membrane translocation of CPPs.

Despite many biophysical studies of CPPs in membrane-mimetic environments, little site-specific high-resolution structural information of membrane-bound CPPs is yet available. Our recent studies of membrane-bound penetratin through solid-state NMR <sup>13</sup>C chemical shifts suggested an unusual turn-rich conformation at physiological temperature (14), whose functional role is still unclear. Moreover, the penetratin conformation was found to depend on the temperature: in the gel phase of the membrane, penetratin adopts a  $\beta$ -strand conformation, while in the liquid-crystalline phase, random coil chemical shifts were observed for

<sup>†</sup>This work was supported by Grant GM066976 from the National Institutes of Health (to M.H.).

\*Corresponding author. Tel: 515-294-3521. Fax: 515-294-0105. E-mail: mhong@iastate.edu.

Abbreviations: CPP, cell-penetrating peptide; DMPC, 1,2-dimyristoyl-sn-glycero-3-phosphatidylcholine; DMPG, 1,2-dimyristoyl-sn-glycero-3-phosphatidylglycerol; POPC, 1-palmitoyl-2-oleoyl-sn-glycero-3-phosphatidylcholine; POPE, 1-palmitoyl-2-oleoyl-sn-glycero-3-phosphoethanolamine; POPG, 1-palmitoyl-2-oleoyl-sn-glycero-3-phosphatidylglycerol; MAS, magic-angle spinning; CP, cross-polarization; DARR, dipolar-assisted rotational resonance; INADEQUATE, incredible natural abundance double-quantum transfer experiment; HETCOR, heteronuclear correlation; DIPSHIFT, dipolar chemical shift correlation; REDOR, rotational echo double-resonance; fwhm, full width at half-maximum.

most labeled sites except for an Arg (14). To further elucidate how conformation underlies the mechanism of CPPs, and to examine the diversity of the structure–function relation for this class of peptides, we have now investigated the structure and dynamics of the hexa-Arg CPP domain of the HIV TAT protein (residues 48–60), whose potent CPP activities have been extensively characterized (15–17). Using solid-state NMR, we have determined the conformation, dynamics, depth of insertion, and lipid interaction of TAT(48–60) in anionic lipid membranes, which led us to propose a structural basis for the translocation mechanism of this peptide.

## MATERIALS AND METHODS

**Membrane Sample Preparation.** TAT(48–60) (GRKKR RQRRR PPQ-CONH<sub>2</sub>) was synthesized using standard solid-phase Fmoc chemistry and purified by HPLC to >95% purity. Uniformly <sup>13</sup>C, <sup>15</sup>N-labeled Lys, Gln, Arg, and Pro were incorporated at residues 4, 7, 8, and 11 of the peptide, respectively, in singly labeled samples. A <sup>13</sup>C, <sup>15</sup>N-Ile<sub>3</sub>-labeled penetratin sample (RQIKI WFQNR RMKW KK-CONH<sub>2</sub>) bound to DMPC/DMPG bilayers (13) was also used for the <sup>1</sup>H  $T_{1\rho}$  experiment to compare with the TAT peptide. All lipids, including DMPC, DMPG, POPC, POPE, and POPG, were purchased from Avanti Polar Lipids (Alabaster, AL). Most experiments were conducted on hydrated DMPC/DMPG (8:7 mol ratio) membranes. The high-melting DMPC/DMPG mixture allows the peptide to be immobilized at moderate low temperatures to facilitate distance and chemical shift measurements. The low-melting unsaturated lipids (POPC, POPE, and POPG) were used in aligned membrane samples since they are more easily hydrated and aligned at ambient temperature. We chose phosphatidylglycerol (PG) instead of phosphatidylserine (PS), which is the anionic lipid of eukaryotic cell membranes, for our samples in order to facilitate comparison with the large literature of CPP studies in model membranes. Eukaryotic cell membranes contain ~10% anionic lipids (18), which is much less than the ~50% charge density used in this work. However, the cationic TAT is most likely clustered in the anionic-lipid-rich regions of the biological membrane during translocation, so the current model membrane is still relevant for understanding the translocation mechanism.

Hydrated membrane samples were prepared by aqueous phase mixing. DMPC and DMPG (8:7 mol ratio) lipids were mixed in chloroform and dried under a stream of N<sub>2</sub> gas. The lipid mixture was further lyophilized overnight to obtain a homogeneous dry powder, which was then suspended in 2 mL of phosphate buffer (5.8 mM NaH<sub>2</sub>PO<sub>4</sub> and 4.2 mM Na<sub>2</sub>HPO<sub>4</sub>, pH = 7.0) and freeze-thawed eight times. The resulting lipid vesicle solution was added to the peptide solution to obtain a peptide:lipid molar ratio of 1:15. After incubation overnight, the solution was centrifuged at 55000 rpm for 4 h at 4–6 °C to obtain a wet pellet. The pellet was slowly dried to a hydration level of ~40 wt % and then packed into a 4 mm MAS rotor for NMR experiments. Over 95% of the peptide was bound to the lipids as checked by UV-vis spectrometry. The POPE/POPG-bound TAT sample was prepared similarly.

Oriented membranes were prepared on thin glass plates using an organic solvent protocol described before (19). The dry lipid/peptide film (~1 mg) on each glass plate was first hydrated by directly dropping 1 μL of water on each plate, giving a hydration level of ~50%. The hydrated glass plates were then kept in a 97% humidity chamber containing saturated K<sub>2</sub>SO<sub>4</sub> solution at room temperature for 4–5 days before NMR measurements. Samples with TAT concentrations at 1%, 2%, 4%, and 8% were prepared

to determine the degree of membrane disorder induced by the peptide. Three series of lipid membranes, neutral POPC, anionic POPC/POPG (8:7), and anionic POPE/POPG (8:7), were prepared.

**Solid-State NMR Experiments.** All solid-state NMR experiments were carried out on a Bruker DSX-400 (9.4 T) spectrometer (Karlsruhe, Germany) operating at 400.5 MHz for <sup>1</sup>H, 100.7 MHz for <sup>13</sup>C, and 162.1 MHz for <sup>31</sup>P. A triple-resonance <sup>1</sup>H/<sup>13</sup>C/<sup>31</sup>P 4 mm magic-angle spinning (MAS) probe was used for <sup>13</sup>C–<sup>31</sup>P REDOR experiments, while a double-resonance <sup>1</sup>H/X MAS probe was used for other MAS experiments. Low temperature was achieved using a Kinetics Thermal System XR air-jet sample cooler (Stone Ridge, NY). All experimental temperatures refer to the sample temperature indicated by the probe thermocouple and are estimated to be within 1° of the actual sample temperature since no fast spinning nor high-salt samples were used in this work. Typical 90° pulse lengths of <sup>13</sup>C, <sup>15</sup>N, and <sup>31</sup>P were 5 μs, and typical <sup>1</sup>H decoupling field strengths were 75 kHz at low temperature and 50 kHz at ambient temperature. <sup>13</sup>C and <sup>15</sup>N chemical shifts were calibrated respectively to the α-Gly <sup>13</sup>C resonance at 176.49 ppm on the TMS scale and <sup>15</sup>N-acetylvaline (NAV) at 122 ppm on the ammonium scale. <sup>31</sup>P chemical shifts were referenced to the hydroxyapatite signal at 2.73 ppm for unoriented samples and to the signal of 98% phosphoric acid at 0 ppm for oriented samples.

<sup>13</sup>C and <sup>15</sup>N cross-polarization (CP) MAS experiments were conducted using CP contact times of 0.5–1.5 ms. One-dimensional double-quantum (DQ) filtered <sup>13</sup>C MAS spectra were measured at 233 K using SPC-5 for <sup>13</sup>C–<sup>13</sup>C dipolar recoupling (20). When extracting full widths at half-maximum, we took care to use appropriate line broadening that is less than the intrinsic line widths of the signals at the specific temperatures.

Two 2D <sup>13</sup>C–<sup>13</sup>C correlation experiments, dipolar-assisted rotational resonance (DARR) (21) and the DQ dipolar INADEQUATE experiment (22), were used to assign the TAT <sup>13</sup>C chemical shifts at low temperature. The INADEQUATE experiment suppresses the natural abundance lipid <sup>13</sup>C signals and gives relatively well-resolved peptide <sup>13</sup>C resonances. The SPC-5 sequence was used for DQ excitation and reconversion. The INADEQUATE spectra were measured at 233 K under 5333 Hz MAS.

2D <sup>13</sup>C–<sup>1</sup>H heteronuclear correlation (HETCOR) experiments without <sup>1</sup>H spin diffusion were used to assign <sup>1</sup>H and <sup>13</sup>C chemical shifts of TAT at ambient temperatures. No <sup>1</sup>H decoupling was applied during the evolution period; thus only signals of highly dynamic species can survive in the spectra. The experiments were conducted either with or without <sup>1</sup>J<sub>CH</sub> decoupling for the  $t_1$  period, by the presence or absence of a <sup>13</sup>C 180° pulse in the middle of the  $t_1$  period. The pulse sequence of the <sup>1</sup>J<sub>CH</sub>-decoupled 2D HETCOR experiment was shown in Figure 2a. The non-<sup>1</sup>J<sub>CH</sub> decoupled HECTOR was conducted at 5 kHz MAS while the <sup>1</sup>J<sub>CH</sub> decoupled HETCOR experiments were carried out under 7–8 kHz MAS at 303 K, in the liquid-crystalline phase of the DMPC/DMPG membrane. For <sup>1</sup>H spin diffusion experiments probing the interaction of TAT with lipids and water, we used a similar HETCOR sequence but with the addition of a <sup>1</sup>H spin diffusion mixing period after  $t_1$  (23). These experiments were carried out under 5 kHz MAS at 303 K.

<sup>13</sup>C–<sup>1</sup>H and <sup>15</sup>N–<sup>1</sup>H order parameters were measured using the 2D dipolar chemical shift correlation (DIPSHIFT) experiment with dipolar doubling (24, 25). The experiments were conducted at 303 K under slow spinning rates of 2800 and 3401 Hz. <sup>1</sup>H homonuclear decoupling was achieved using semiwindowless MREV-8 with a <sup>1</sup>H 105° pulse length of 4.0 μs (26). Small asymmetry in the

$t_1$  curves was fit using an apparent  $T_2$  relaxation factor. The best-fit couplings were divided by the theoretical scaling factor, 0.47, of semiwindowless MREV-8 and a factor of 2 for doubling to give the true X–H dipolar couplings. The order parameters,  $S_{XH}$ , were calculated as the ratio of the true coupling with the rigid-limit one-bond X–H dipolar coupling. The rigid limit value was taken as 22.7 kHz for C–H and 10.6 kHz for N–H dipolar coupling, respectively.

$^1\text{H}$  rotating-frame spin–lattice relaxation times ( $T_{1\rho}$ ), which reflect microsecond time scale motions that are important for biological membranes, were measured using a  $^{13}\text{C}$ -detected  $^1\text{H}$  Lee–Goldburg spin-lock sequence with an effective  $^1\text{H}$  field strength of 61.2 kHz (27). The experiments were conducted at 303 K under 7 kHz MAS.

$^{13}\text{C}$ – $^{31}\text{P}$  rotational-echo double-resonance (REDOR) experiments were carried out under 4 kHz MAS at 230 K, where both the lipids and the peptide were immobilized. A  $^{31}\text{P}$  180° pulse length of 9  $\mu\text{s}$  was used to achieve complete inversion of the broad  $^{31}\text{P}$  spectral width. A frequency-selective version of REDOR (28) was used to measure the distance of  $\text{Ca}$  to  $^{31}\text{P}$ . A 1 ms  $^{13}\text{C}$  Gaussian 180° pulse centered at the  $^{13}\text{C}$  resonance of interest was used to remove the  $J$ -coupling between the on-resonance  $\text{Ca}$  and its directly bonded  $^{13}\text{C}$  spins. Two-spin simulations were used to fit the  $^{13}\text{C}$ – $^{31}\text{P}$  REDOR data. Although multiple  $^{31}\text{P}$  spins are present on the membrane surface, the average  $^{31}\text{P}$  density on the membrane surface (10 Å spacing between  $^{31}\text{P}$  atoms) is sufficiently low that when the REDOR dephasing is fast, corresponding to two-spin  $^{13}\text{C}$ – $^{31}\text{P}$  distances of ~5 Å or less, two-spin simulations report the correct distance of the  $^{13}\text{C}$  to a single  $^{31}\text{P}$  (29). When the dephasing is slow, comparison of multispin and two-spin simulations indicated that the two-spin distance is effectively the vertical distance between the  $^{13}\text{C}$  and the  $^{31}\text{P}$  plane, thus reporting the depth of the  $^{13}\text{C}$  spin (29).

Due to overlap with the lipid  $^{13}\text{CO}$  signals, the  $^{13}\text{CO}$ – $^{31}\text{P}$  REDOR data were corrected for the natural abundance lipid background (13) using the equation  $(S/S_0)_{\text{observed}} = 0.79(S/S_0)_{\text{peptide}} + 0.21(S/S_0)_{\text{lipid}}$ , where the weight fractions were calculated based on the peptide:lipid molar ratio of 1:15. The lipid  $^{13}\text{CO}$ – $^{31}\text{P}$  REDOR dephasing was previously measured using POPC lipids (29). The  $\text{Pro}_{11}$   $\text{Ca}$  REDOR was similarly corrected for the small percentage of overlapping natural abundance lipid  $\text{Ca}$  signal, whose distance to  $^{31}\text{P}$  is fixed at 2.9 Å. To fit the Arg  $\text{C}\zeta$  REDOR data, which shows heterogeneous couplings, we used two distances in the simulation, where the long and short distances were each incremented at 0.1 Å steps within physically allowed ranges (13). The best fit was obtained as the lowest rmsd between the data and simulations. Supporting Information Table S1 summarizes the main conditions of all the experiments carried out in this work.

## RESULTS

**Random Coil Conformation and High Mobility of TAT in Lipid Bilayers.** We first examined the conformation of TAT in DMPC/DMPG membranes using  $^{13}\text{C}$  and  $^{15}\text{N}$  chemical shifts. Four uniformly  $^{13}\text{C}$ ,  $^{15}\text{N}$ -labeled residues, Lys<sub>4</sub>, Gln<sub>7</sub>, Arg<sub>8</sub>, and Pro<sub>11</sub>, were singly incorporated into the peptide. Figure 1 shows representative 2D  $^{13}\text{C}$ – $^{13}\text{C}$  correlation spectra of Lys<sub>4</sub>- and Arg<sub>8</sub>-labeled TAT in the gel phase of the membrane at 233 K. Broad  $\text{Ca}$  and  $\text{C}\beta$  peaks with line widths of 4.0–5.1 ppm were observed, indicating significant conformational heterogeneity. When the lipid  $^{13}\text{C}$  signals were removed by a double-quantum (DQ) filter, more than one set of  $^{13}\text{C}$  chemical shifts was found for some of

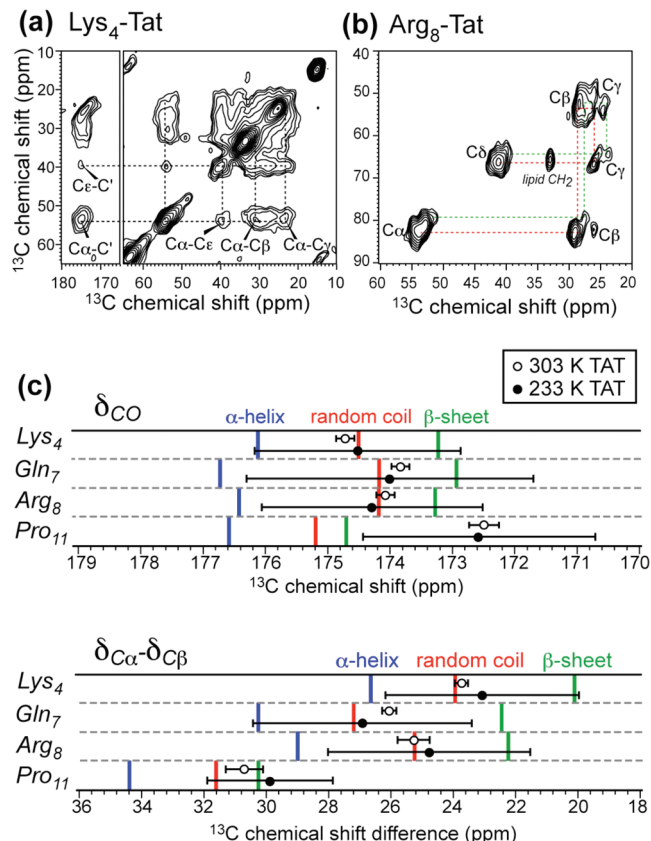


FIGURE 1:  $^{13}\text{C}$  chemical shifts of HIV TAT(48–60) in DMPC/DMPG (8:7) bilayers. (a) 2D  $^{13}\text{C}$ – $^{13}\text{C}$  DARR spectrum of Lys<sub>4</sub>-TAT at 233 K, measured with a mixing time of 30 ms. (b) 2D INADEQUATE spectrum of Arg<sub>8</sub>-TAT at 233 K. (c) TAT  $^{13}\text{C}$  chemical shifts at 303 K (open circles) and 233 K (closed circles) compared to database values for various secondary structures (31). Error bars indicate the fwhm. The  $\text{Ca}$ – $\text{C}\beta$  chemical shift difference was used as a marker of secondary structure (58).

the  $^{13}\text{C}$  sites in Lys<sub>4</sub>, Gln<sub>7</sub>, and Arg<sub>8</sub> (Figure 1b), suggesting that the conformational distribution may be more complex than a single Gaussian. Chemical shift multiplicity for the same domain in the intact TAT protein was also observed in solution and was postulated to result from transient folding events of the protein (30). When the chemical shifts of the dominant peaks of membrane-bound TAT were compared with random coil values from protein databases (31), we found most residues to exist in a random coil state (Figure 1c). The only exception is Pro<sub>11</sub>, which is known to be predisposed to  $\beta$ -strand conformation by the imine side chain.

To examine if the random coil chemical shifts of TAT at low temperature were caused by the gel-phase disorder of the membrane, we measured the TAT  $^{13}\text{C}$  chemical shifts in the liquid-crystalline phase of the membrane at 303 K using 2D  $^1\text{H}$ – $^{13}\text{C}$  correlation experiments. Even in the absence of  $^1\text{H}$ – $^1\text{H}$  homonuclear decoupling, we observed extremely narrow  $^1\text{H}$  and  $^{13}\text{C}$  line widths and resolved  $^1J_{\text{CH}}$  splittings in the  $^1\text{H}$  dimension (Figure 2b): the  $^{13}\text{C}$  line widths were 0.3–0.4 ppm while the undecoupled  $^1\text{H}$  line widths were 0.15–0.30 ppm. Thus, fast isotropic motion largely averaged the  $^1\text{H}$ – $^1\text{H}$  dipolar couplings, giving well-resolved  $^1\text{H}$  peaks even without homonuclear decoupling. As a comparison, in the HETCOR spectrum (data not shown) of Ile<sub>3</sub>-labeled penetratin with  $^1J_{\text{CH}}$  decoupling, no peptide  $^1\text{H}$  peaks survived, indicating penetratin has slower motion than TAT. Most importantly, the TAT  $^{13}\text{C}$  chemical shifts remained at the random coil positions, close to the center of the broad peaks

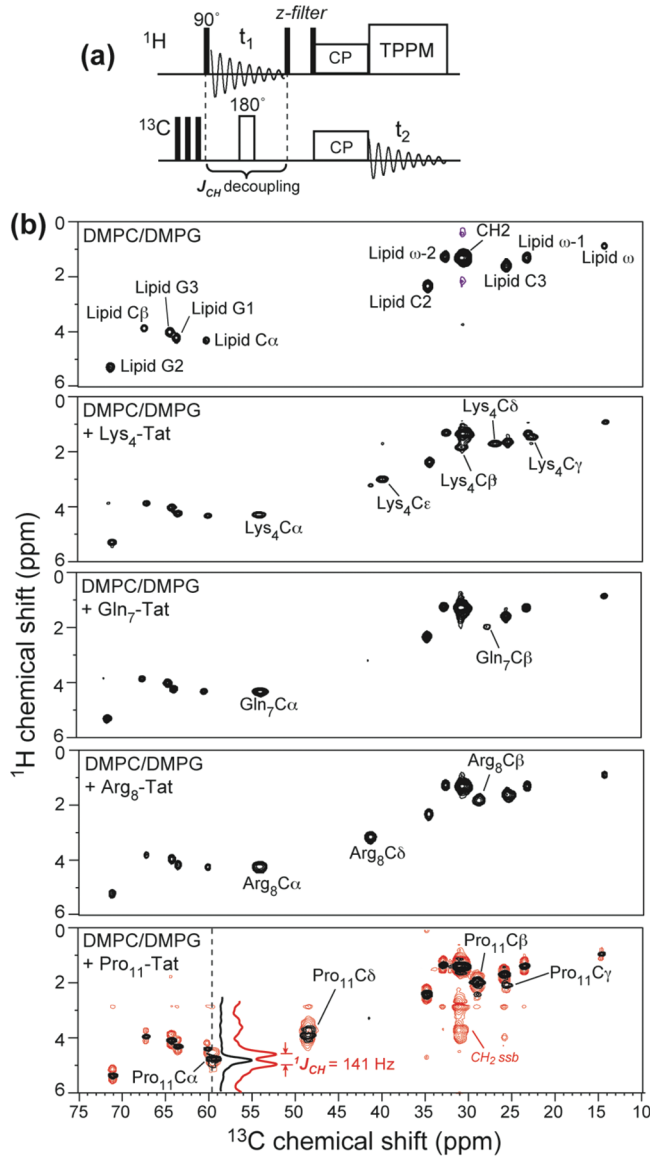


FIGURE 2: 2D  $^1\text{H}$ – $^{13}\text{C}$  HETCOR spectra of TAT in DMPC/DMPG bilayers at 303 K. (a) Pulse sequence of  $^1\text{J}_{\text{CH}}$ -decoupled 2D HETCOR experiment. No  $^1\text{H}$  homonuclear decoupling was applied during  $t_1$ ; thus only highly dynamic molecules can exhibit  $^1\text{H}$ – $^{13}\text{C}$  cross-peaks. (b)  $^1\text{J}_{\text{CH}}$ -decoupled HETCOR spectra (black) of the DMPC/DMPG membrane without and with various site-specifically labeled TAT. The spectrum in red in the bottom panel is the HETCOR spectrum of Pro<sub>11</sub>-TAT without  $^1\text{J}_{\text{CH}}$  decoupling. A 141 Hz  $^1\text{J}_{\text{CH}}$  splitting of the Pro<sub>11</sub> Cα peak was observed. The Cα  $^1\text{H}$  cross section was compared between the  $^1\text{J}_{\text{CH}}$ -decoupled and undecoupled spectra.

at low temperature (Figure 1c). Thus, TAT undergoes near-isotropic motion at high temperature, with an average conformation approaching the random coil. This result is consistent with circular dichroism data of TAT in POPC/POPG vesicles, which also suggested a random coil structure similar to that in buffer (32).

To observe how the narrow line widths of TAT at high temperature transition to broad line widths at low temperature, we measured the 1D  $^{13}\text{C}$  and  $^{15}\text{N}$  spectra of TAT as a function of temperature (Table 1). Figure 3a,b shows  $^{13}\text{C}$  and  $^{15}\text{N}$  spectra of Arg<sub>8</sub>-labeled TAT bound to DMPC/DMPG bilayers from 303 to 233 K. The Arg<sub>8</sub> signals were sharp at 303 K; the limiting  $^{13}\text{C}$  line widths were sufficiently small that  $^{13}\text{C}$ – $^{13}\text{C}$  scalar splittings of ~40 Hz were observed for many sites such as Cα. The peptide

Table 1:  $^1\text{H}$ ,  $^{13}\text{C}$ , and  $^{15}\text{N}$  Chemical Shifts (ppm) of Labeled Residues of TAT in DMPC/DMPG Bilayers at 303 and 233 K

residue	site	303 K	233 K	random coil values (31)
Lys <sub>4</sub>	CO	174.7	174.5	174.5
	C $\alpha$	54.4	54.3	54.7
	C $\beta$	30.9	31.3	30.8
	C $\gamma$	22.8	22.9	
	C $\delta$	27.2	26.3	
	C $\epsilon$	40.2	39.7	
	H $\alpha$	4.29		4.28
	H $\beta$	1.82		
	H $\gamma$	1.45		
	H $\delta$	1.69		
Gln <sub>7</sub>	CO	173.8	174.0	174.2
	C $\alpha$	53.8	53.8	54.2
	C $\beta$	27.8	26.7	27.0
	C $\gamma$	32.0	33.3	
	C $\delta$	178.4	177.9	
	H $\alpha$	4.37		4.26
	H $\beta$	2.01		
	N $\alpha$	123.1	122.2	118.9
	N $\epsilon$	85.4	83.2	
	N $\eta$	73.0	71.3	
Arg <sub>8</sub>	CO	174.1	174.3	174.2
	C $\alpha$	54.2	53.4	54.3
	C $\beta$	28.9	28.7	28.8
	C $\gamma$	25.2	25.4	
	C $\delta$	41.5	41.0	
	C $\zeta$	157.7	156.9	
	H $\alpha$	8.40		8.17
	H $\beta$	4.31		4.33
	H $\gamma$	1.87		
	H $\delta$	1.64		
		3.22		
Pro <sub>11</sub>	N $\alpha$	138.3	136.9	
	CO	172.5	172.6	175.2
	C $\alpha$	59.7	58.6	61.8
	C $\beta$	29.0	28.7	30.2
	C $\gamma$	25.4	25.5	
	C $\delta$	48.6	48.3	
	H $\alpha$	4.68		4.41
	H $\beta$	1.92		
	H $\gamma$	2.00		
	H $\delta$	3.82		

signals became undetectable around 283 K and became broad and strong at 233 K, with 3.5–4.8 ppm line widths for  $^{13}\text{C}$  and a 12 ppm line width for N $\alpha$ . Similar trends were observed for the other labeled residues. For the backbone C $\alpha$ , the low-temperature line width of Arg<sub>8</sub> covers the entire range of helix to sheet conformations (Figure 3c). We further compared the TAT line widths to several other membrane peptides, including penetratin, the  $\beta$ -sheet antimicrobial peptide PG-1 (29), and the  $\alpha$ -helical influenza M2 transmembrane peptide (33). Among these peptides, TAT exhibits the narrowest line widths at high temperature and the largest line widths at low temperature (Figure 3d), indicating that TAT undergoes faster exchange among a wider range of conformations at high temperature, thus giving rise to sharp signals averaged at the random coil chemical shifts. Lowering the temperature freezes the motion and captures all conformation-dependent chemical shifts. Thus, the broad low-temperature line widths reflect the large conformational space sampled by TAT. While it is difficult to quantify the exact conformational distribution, compared to the structurally defined  $\beta$ -sheet PG-1 and  $\alpha$ -helical M2, the TAT structure is almost completely random. Comparison with PG-1 and M2 also indicates that the contribution of gel-phase

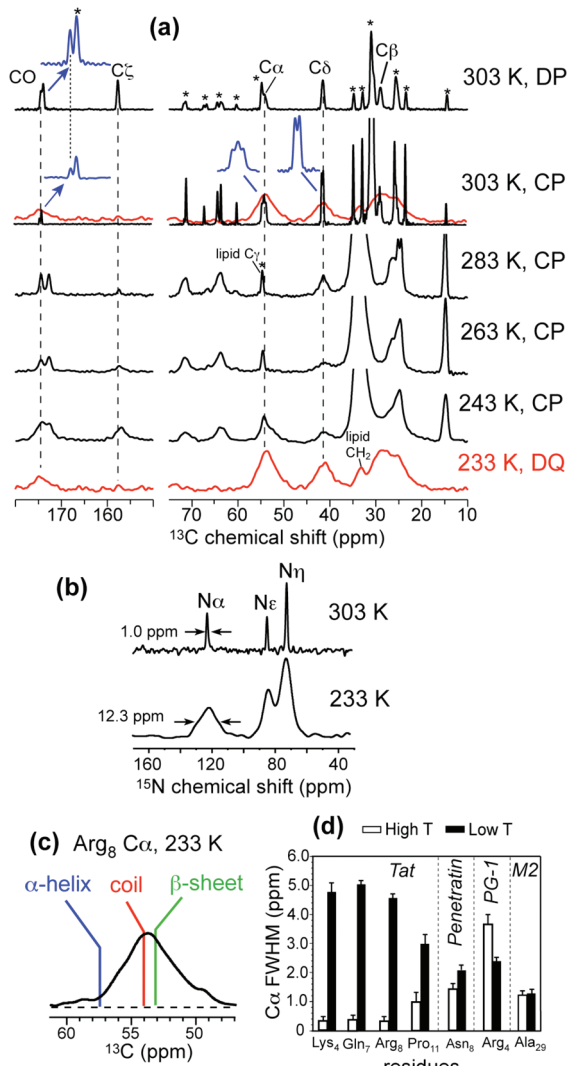


FIGURE 3: Temperature-dependent TAT line widths in DMPC/DMPG membranes. (a) <sup>13</sup>C MAS spectra from 303 to 233 K for Arg<sub>8</sub>-TAT. Stars denote lipid peaks. Most spectra were measured by cross-polarization (CP). A 303 K spectrum was measured by <sup>13</sup>C direct polarization (DP). A 233 K <sup>13</sup>C DQ-filtered spectrum gives pure peptide peaks and line widths. <sup>13</sup>C–<sup>13</sup>C *J* splittings were resolved for some peaks at 303 K, as shown in expanded regions in blue. (b) <sup>15</sup>N spectra of Arg<sub>8</sub>-TAT at 303 K (by DP) and 233 K (by CP). (c) The C<sub>α</sub> peak of Arg<sub>8</sub> at 233 K from the DQ spectrum spans the chemical shift range for canonical secondary structures. (d) Comparison of C<sub>α</sub> line widths of TAT, penetratin, PG-1, and the influenza M2 peptide in lipid bilayers at high and low temperatures.

membrane disorder is minor compared to the intrinsic disorder of the peptide. Furthermore, the possibility that freezing changed the TAT conformation can be ruled out, since the average chemical shift frequencies were unchanged between high and low temperatures (with the slight exception of Pro<sub>11</sub> C<sub>α</sub>).

To quantify the dynamics of TAT in the lipid membrane, we measured <sup>13</sup>C–<sup>1</sup>H and <sup>15</sup>N–<sup>1</sup>H dipolar couplings and the corresponding order parameters at 303 K using 2D DIPSHIFT experiments. Order parameters indicate the amplitude of motion. A maximum order parameter of 1 corresponds to the rigid limit while a minimum order parameter of 0 indicates large-amplitude, isotropic motion. Figure 4 shows representative dipolar coupling data of the membrane-bound TAT. Low order parameters of 0.14–0.20 were found for the peptide backbone (Table 2), comparable to those of the middle portion of the lipid molecules (34),

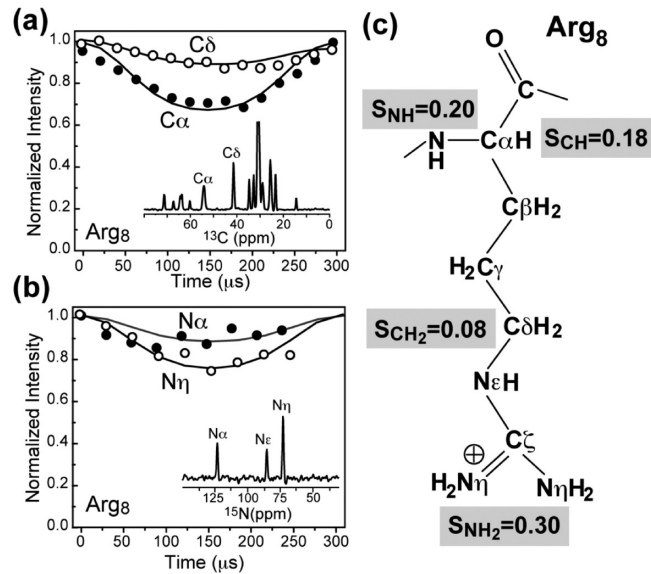


FIGURE 4: C–H and N–H dipolar couplings of Arg<sub>8</sub>-TAT in DMPC/DMPG membranes at 303 K. (a) C<sub>α</sub> and C<sub>δ</sub> C–H DIPSHIFT curves. (b) N<sub>α</sub> and N<sub>η</sub> N–H DIPSHIFT curves. (c) Arg<sub>8</sub> order parameters from the measured dipolar couplings. The lowest order parameters were observed for the middle of the side chain, while the guanidinium moiety and the backbone exhibit higher order parameters.

Table 2: <sup>13</sup>C–<sup>1</sup>H and <sup>15</sup>N–<sup>1</sup>H Dipolar Couplings (kHz) and Order Parameters of TAT in DMPC/DMPG Membranes at 303 K

residue	site	$\delta$ (ppm)	XH <sub>n</sub>	$\omega_{XH}^a$	S <sub>XH</sub>
Arg <sub>8</sub>	N <sub>α</sub>	123.1	NH	2.13	0.20
	N <sub>η</sub>	73.0	NH <sub>2</sub>	3.19	0.30
	C <sub>α</sub>	54.2	CH	4.09	0.18
	C <sub>β</sub>	28.9	CH <sub>2</sub>	3.41	0.15
	C <sub>δ</sub>	41.4	CH <sub>2</sub>	1.82	0.08
Pro <sub>11</sub>	C <sub>α</sub>	59.7	CH	3.18	0.14
	C <sub>β</sub>	28.9	CH <sub>2</sub>	3.86	0.17
	C <sub>δ</sub>	48.7	CH <sub>2</sub>	4.54	0.20
lipids	C <sub>α</sub>	60.3	CH <sub>2</sub>	2.72	0.12
	G <sub>2</sub>	71.4	CH	4.31	0.19
	C <sub>2</sub>	34.7	CH <sub>2</sub>	4.77	0.21
	(CH <sub>2</sub> ) <sub>n</sub>	31.0	CH <sub>2</sub>	5.68	0.25

<sup>a</sup> $\omega_{XH}$  is the true dipolar couplings after taking into account various scaling factors in the pulse sequence. The rigid-limit couplings used for calculating the order parameters are 10.6 kHz for N–H and 22.7 kHz for C–H dipolar couplings.

indicating that the peptide undergoes large-amplitude motion. Interestingly, the Arg<sub>8</sub> order parameters decrease from N<sub>α</sub> ( $S_{NH} = 0.20$ ) to C<sub>δ</sub> ( $S_{CH} = 0.08$ ) but then reverse the trend and increase to N<sub>η</sub> ( $S_{NH} = 0.30$ ), indicating that two relatively rigid ends of the residue flank a more mobile aliphatic middle (Figure 4c). The larger order parameters of the guanidinium moiety immediately suggest stabilizing interactions with the lipid headgroups. TAT also exhibits long <sup>1</sup>H  $T_{1ρ}$  relaxation times of 10–30 ms (Table 3), indicating that the large-amplitude motions occur at rates far exceeding  $10^6$  s<sup>-1</sup>.

*Interaction of TAT with Lipid Membranes.* To probe whether TAT binding causes membrane disorder, we measured <sup>31</sup>P spectra of oriented lipid bilayers of several compositions in the presence of increasing amounts of the peptide. Figure 5 shows the effects of TAT on both the neutral zwitterionic POPC membrane and two anionic membranes, POPC/POPG (8:7) and POPE/POPG

(8:7). Up to 8 mol % peptide, the POPC and POPC/POPG membranes remain largely well ordered, as shown by the high 0° peak at ~30 ppm and the low 90° peak of the powder pattern at -15 ppm, which is indicative of misalignment of the membrane. The lack of an isotropic peak at 0 ppm indicates that the membrane remains lamellar and intact. For the POPE/POPG membrane, higher powder intensities were observed compared to the other two membranes, but the isotropic peak is still absent. The lack of membrane disruption was further confirmed by static  $^{31}\text{P}$  spectra of unoriented DMPC/DMPG and POPE/POPG membranes containing 6% TAT, where regular uniaxial powder line shapes were observed (Figure 5b). The minor isotropic peaks were attributed to the phosphate buffer. The lack of isotropic disorder is consistent with previously reported  $^{31}\text{P}$  NMR spectra of unoriented POPC/POPG (3:1) membranes (32) containing TAT and is also consistent with the ability of this cell-penetrating peptide to cross the membrane without damaging its integrity.

*Depth of Insertion of TAT in Lipid Bilayers from  $^1\text{H}$  Spin Diffusion.* To determine how deeply TAT is inserted into the lipid bilayer, we carried out  $^{13}\text{C}$ -detected  $^1\text{H}$  spin diffusion

Table 3:  $^1\text{H} T_{1\rho}$  Relaxation Times (ms) of TAT and Penetratin in DMPC/DMPG Membranes at 303 K, Measured with a  $^1\text{H}$  Effective Spin-Lock Field of 61.2 kHz

peptide	residue	site	$T_{1\rho}$ (ms)
TAT(48–60)	Arg <sub>8</sub>	C $\alpha$	11.6
		C $\beta$	11.3
		C $\delta$	29.3
	Pro <sub>11</sub>	C $\alpha$	14.9
		C $\beta$	8.8
		C $\delta$	7.0
penetratin	Ile <sub>3</sub>	C $\alpha$	3.0
		C $\delta$	4.9
		C $\epsilon$	6.2

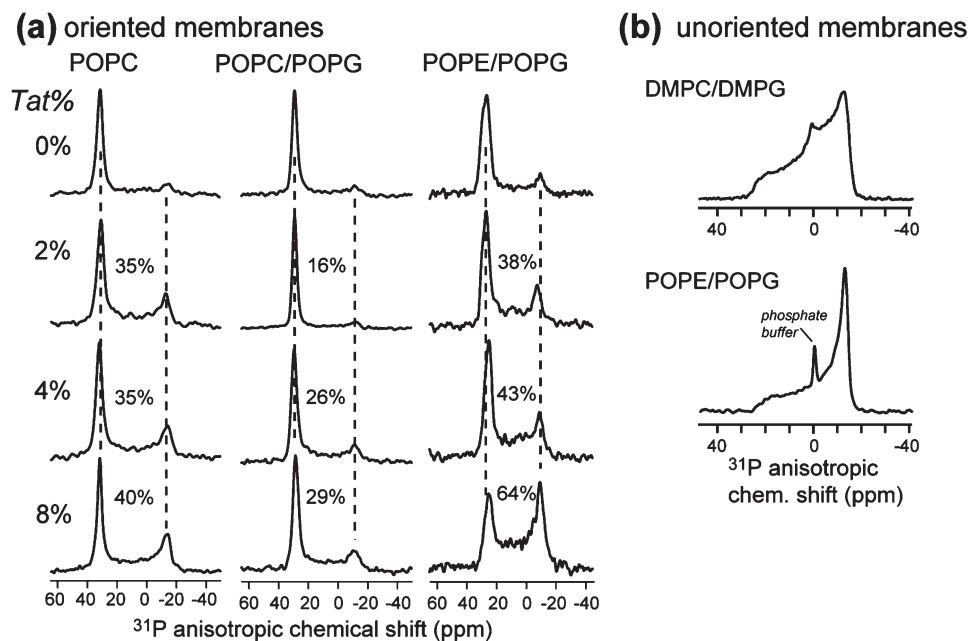


FIGURE 5: Effects of TAT on the membrane structure. (a) Static  $^{31}\text{P}$  spectra of glass-plate oriented lipid membranes with varying mole concentrations of TAT. Three membrane compositions, POPC, POPC/POPG (8:7), and POPE/POPG (8:7), were examined. The percentage of intensity in the 12 to -27 ppm range is indicated for each spectrum to denote the amount of membrane disorder. No isotropic signal near 0 ppm was observed in any spectra. (b) Static  $^{31}\text{P}$  spectra of unoriented DMPC/DMPG (8:7) membrane and POPE/POPG (8:7) membranes containing 6 mol % TAT. The isotropic peak at 1.6 ppm is the phosphate buffer peak. All  $^{31}\text{P}$  spectra were measured at 296 K.

experiments from water and lipids to the peptide (23). The distance between the source protons and protein protons determines the intensities of the intermolecular cross-peaks. Since TAT is similarly mobile as lipids at ambient temperature, the dipolar-mediated  $^1\text{H}$  spin diffusion process is similarly inefficient in the peptide as in the soft lipid matrix. Therefore, spin diffusion cross-peak intensities depend on the distances of individual residues from the source protons. The site-specific nature of the depth information for the mobile TAT differs from the case of large immobile membrane proteins, where rapid spin diffusion within the protein largely removes the site resolution of the depth, and only the shortest distance between the protein and the source protons can be obtained (23).

Figure 6 shows representative  $^{13}\text{C}$ -detected  $^1\text{H}$  spin diffusion spectra of Arg<sub>8</sub>- and Pro<sub>11</sub>-TAT, measured with a  $^1\text{H}$  spin diffusion mixing time of 225 and 144 ms, respectively. Weak cross-peaks were observed between the lipid chain CH<sub>2</sub> protons at 1.3 ppm and the peptide  $^{13}\text{C}$  signals. The mixing time of 100–200 ms is modest for the highly dynamic TAT with low spin diffusion coefficients. For comparison, immobilized DNA bound to the surface of cationic lipid membranes showed no cross-peaks with the lipid chain protons until after ~400 ms, even though the spin diffusion coefficient of the rigid DNA rods is much larger than TAT (23). Thus, if TAT were similarly surface-bound as DNA, ~20 Å from the center of the membrane, then it will not exhibit any cross-peaks with the lipid chain protons in the short mixing times used here. Therefore, the presence of the lipid–TAT cross-peaks within the modest mixing time is strong qualitative evidence that TAT binds inside the lipid bilayer rather than lying on the membrane surface.

Figure 6 shows strong water cross-peaks at 4.7 ppm for Arg<sub>8</sub> but not Pro<sub>11</sub>. Figure 7 compares the water region of the  $^{13}\text{C}$ – $^1\text{H}$  2D spectra for all sites studied. Interestingly, all polar residues containing labile protons, Lys<sub>4</sub>, Gln<sub>7</sub>, and Arg<sub>8</sub>, exhibited water cross-peaks, while the hydrophobic Pro<sub>11</sub> without any exchangeable

protons did not. This difference indicates that hydrogen exchange is necessary for water–protein spin diffusion cross-peaks to occur, consistent with many recent studies of the mechanism of water–protein magnetization transfer (35–37). Thus, Pro<sub>11</sub> is not necessarily further away from water than the other residues. Overall, the strong water cross-peaks with the peptide indicate that TAT is not deeply inserted into the bilayer.

The coexistence of water and lipid cross-peaks with TAT is most consistent with a location of the peptide in the glycerol backbone and headgroup region of the membrane. This interfacial location inside the membrane is further supported by the fact that TAT enhanced the water-to-lipid spin diffusion of the

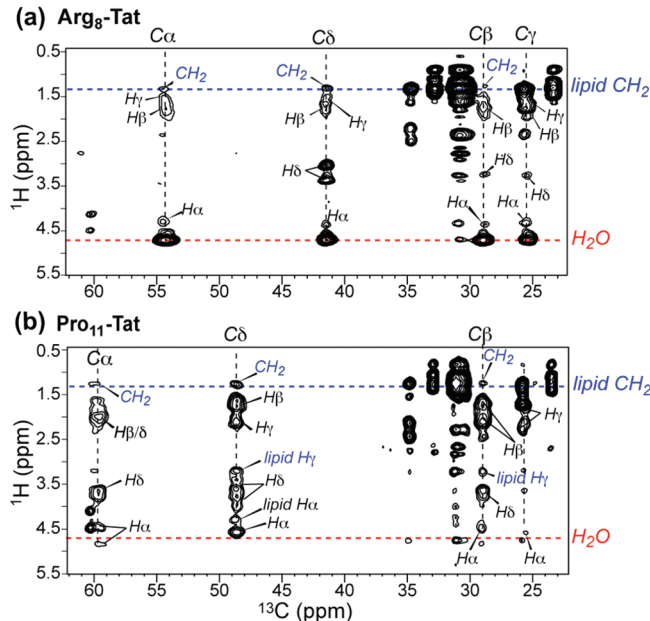


FIGURE 6: (a) 2D <sup>13</sup>C-detected <sup>1</sup>H spin diffusion spectra of DMPC/DMPG-bound TAT at 303 K. (a) Arg<sub>8</sub>-TAT spectrum measured with 225 ms spin diffusion. Water and lipid CH<sub>2</sub> cross-peaks are colored. (b) Pro<sub>11</sub>-TAT spectrum with a mixing time of 144 ms. No water cross-peaks (37) but clear lipid CH<sub>2</sub> cross-peaks were detected.

POPE/POPG membrane. Figure 8 shows that the lipid head-group C $\alpha$  and acyl chain C2 have stronger cross-peaks with water in the presence of TAT than in its absence, which is not possible if TAT were on the surface of the membrane.

The exact distance of TAT to the center of the membrane cannot be quantified by observing cross-peak buildup intensities as a function of mixing time due to the lack of well-calibrated spin diffusion coefficients for dynamic molecules. Nevertheless, one can obtain some insights based on the relative intensities of the water–peptide and lipid–peptide cross-peaks. In ~40% hydrated membrane samples, the number of water protons is about twice the number of lipid CH<sub>2</sub> protons. Previous calibrations of water and lipid chain spin diffusion coefficients indicated that the water spin diffusion coefficient is about 10-fold larger than the lipid chain diffusion coefficient because of the faster translational motion of water (23, 38). Thus, the water–peptide cross-peak should be higher than the lipid–peptide cross-peak even if a residue is at comparable distances to the membrane surface water and to the hydrophobic chains. Thus, the presence of a lipid–TAT cross-peak at all is a strong indication of the membrane-immersed nature of TAT.

*Site-Specific Distances to the Membrane Surface from <sup>13</sup>C–<sup>31</sup>P REDOR.* To confirm the interfacial location of TAT, we carried out <sup>13</sup>C–<sup>31</sup>P distance measurements at low temperature using REDOR. If TAT were inserted into the hydrophobic core of the bilayer, long <sup>13</sup>C–<sup>31</sup>P distances or slow dipolar dephasing would be expected, as is the case for the lipid chain <sup>13</sup>C signal. The REDOR experiments were conducted at ~230 K to completely freeze the dynamics of both the DMPC/DMPG membrane and the peptide. The <sup>31</sup>P spectra at this temperature give a span of 197 ppm (Supporting Information Figure S1), which is the rigid limit for the <sup>31</sup>P chemical shift tensor (29). Figure 9 shows the <sup>13</sup>C–<sup>31</sup>P REDOR data of the backbone and side chain sites of Arg<sub>8</sub> and Pro<sub>11</sub>. Relatively short backbone <sup>13</sup>C–<sup>31</sup>P distances of 5.7–6.6 Å were observed, consistent with the <sup>1</sup>H spin diffusion result that the peptide backbone lies in the glycerol backbone region of the membrane–water interface. Natural abundance lipid signals were corrected for both the

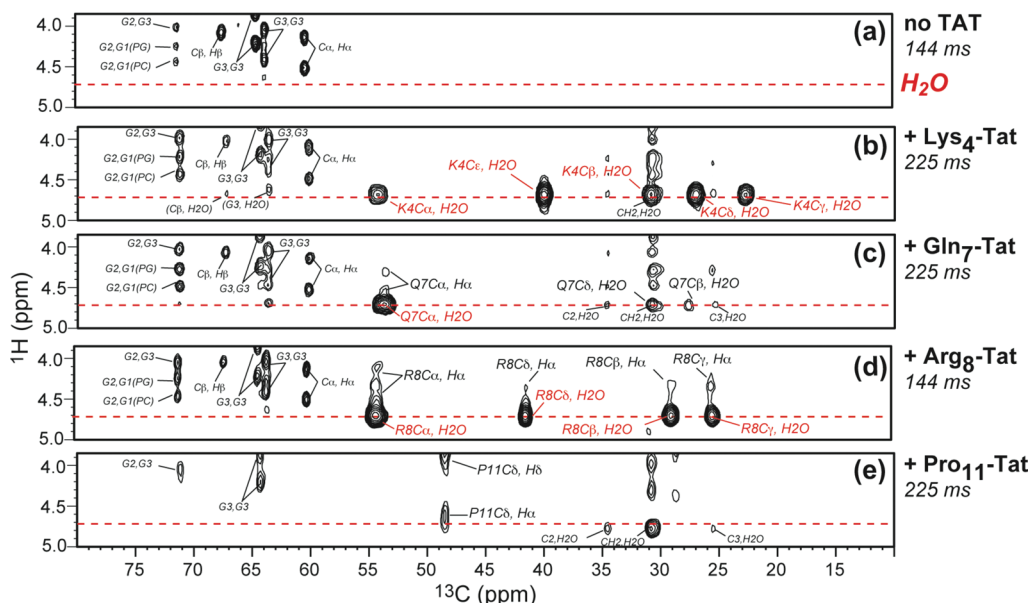


FIGURE 7: 2D <sup>13</sup>C-detected <sup>1</sup>H spin diffusion spectra of DMPC/DMPG (8:7) membranes with and without TAT. (a) Without TAT. (b) With Lys<sub>4</sub>-labeled TAT. (c) With Gln<sub>7</sub>-labeled TAT. (d) With Arg<sub>8</sub>-labeled TAT. Water–peptide cross-peaks were detected in (b)–(d). (e) With Pro<sub>11</sub>-labeled TAT with a mixing time of 225 ms. No Pro<sub>11</sub>–water cross-peaks were observed.

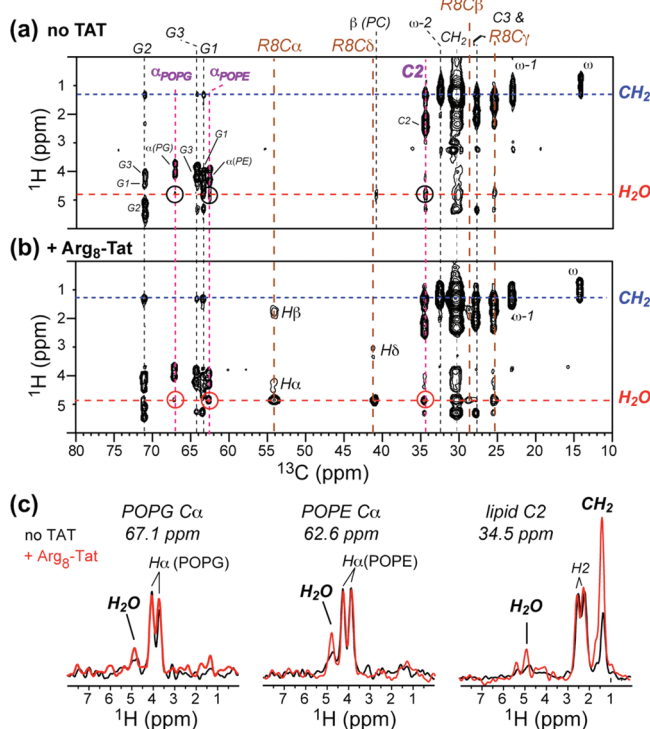


FIGURE 8: 2D  $^{13}\text{C}$ -detected  $^1\text{H}$  spin diffusion spectra of POPE/POPG (8:7) membranes with a mixing time of 144 ms. (a) Without TAT. Only very weak water–lipid cross-peaks were observed. (b) With Arg8-labeled TAT (P/L = 1:15), showing stronger water–lipid cross-peaks. (c)  $^1\text{H}$  cross sections at several lipid  $^{13}\text{C}$  frequencies. The TAT-free spectrum is in black, and the TAT-containing spectrum is in red. TAT enhances the water–lipid cross-peaks, indicating that the peptide is inserted into the membrane. All spectra were measured at 303 K under 5 kHz MAS.

$\text{Arg}_8$  CO peak and the  $\text{Pro}_{11}$  C $\alpha$  peak. For the guanidinium C $\zeta$  of  $\text{Arg}_8$ , a 1:1 combination of 4.1 and 5.5 Å distances fits the data well (Figure 9b). The former is at the lower limit of the possible distance between the guanidinium and the lipid phosphate and places the two groups within hydrogen-bonding contact of each other (29, 39). Thus, the Arg residues in TAT interact with the negatively charged lipid headgroups in a similar fashion to Arg-rich antimicrobial peptides (29, 40). Since the superposition of two distances fits the C $\zeta$  data well, there is no sign of a broad distance distribution, suggesting that guanidinium–phosphate ion pair interaction, rather than the peptide backbone conformation, is the determining factor for the Arg side chain conformation.

## DISCUSSION

*Depth and Thermodynamics of Insertion of TAT into Lipid Membranes.* The  $^1\text{H}$  spin diffusion and  $^{13}\text{C}$ - $^{31}\text{P}$  distance data indicate that TAT binds inside the DMPC/DMPG (8:7) bilayer in the glycerol backbone and headgroup region of the membrane–water interface (Figure 10). This location is consistent with the temperature dependence of the  $^{13}\text{C}$  and  $^{15}\text{N}$  spectra (Figure 3), since exchange broadening of TAT signals coincided with the membrane phase transition. This depth is also consistent with molecular dynamics simulations of TAT and the related CPP penetratin (41, 42).

It is interesting to consider the free energies of TAT insertion into the membrane–water interface. Using the Wimley–White interfacial scale developed for zwitterionic POPC bilayers (43), an energy barrier of about 9 kcal/mol against insertion would be predicted. However, the interfacial scale derived from neutral POPC

bilayers does not account for strong electrostatic attraction between cationic peptides and highly anionic membranes as used in this study. Using isothermal titration calorimetry experiments, Seelig and co-workers characterized the thermodynamics of TAT binding to anionic membranes in detail and found that the free energy of binding of TAT to 25% anionic membranes in 100 mM salt solution was about 80% electrostatic and 20% hydrophobic, with a total Gibbs free energy of  $-5.2$  kcal/mol (32). The NMR samples used here contain less salt (10 mM) and more (~50%) anionic lipids; thus the binding energy should be even more negative or favorable. Similar to TAT, oligoarginine peptides also showed a significant electrostatic component in their binding energies (44).

In addition to the electrostatic attraction,  $^{13}\text{C}$ – $^{31}\text{P}$  REDOR experiments found tight association of the Arg<sub>8</sub> guanidinium group with the lipid phosphates, similar to a number of other Arg-rich CPPs and antimicrobial peptides (13, 29, 40). A C $\zeta$ –P distance of 4–5 Å indicates hydrogen bonding between the guanidinium N–H and the lipid P–O groups. The importance of this hydrogen bonding was demonstrated for the antimicrobial peptide PG-1, where mutation of the guanidinium to dimethylated guanidinium weakened the antimicrobial activity by 3-fold and changed the oligomeric structure and orientation of the peptide in the lipid bilayer (40). Each guanidinium ion can form up to five hydrogen bonds with lipid phosphates or water. Thus, the hexa-Arg TAT can form as many as 30 hydrogen bonds from the Arg side chains. If each hydrogen bond formation gives a favorable free energy change of  $-0.5\text{ kcal/mol}$  (45), then the total free energy change can be as much as  $-15\text{ kcal/mol}$  in favor of binding, which would greatly stabilize TAT at the membrane–water interface. Therefore, the combined electrostatic attraction and hydrogen-bonding effects should be more than sufficient to overcome Born repulsion and facilitate TAT insertion into the glycerol backbone region of the membrane–water interface. An increasing number of MD simulations also pointed out the importance of guanidinium–phosphate and guanidinium–water interactions for reducing the free energy cost of inserting Arg residues into the lipid membrane (42, 46–48).

The location of TAT is deeper than polylysine peptides, which was found by monolayer pressure and area measurements to lie on the surface of anionic lipid monolayers (49). Differences in the experimental conditions as well as the intrinsic membrane affinities of the two peptides most likely account for the observed depth difference. The polylysine measurements were carried out in 33% negatively charged membranes in 100 mM salt (49), while the bilayer samples in the present NMR study contained ~50% anionic lipids and only 10 mM salt. A lower fraction of acidic lipids reduces the electrostatic attraction while a higher salt concentration shields the electrostatic attraction between the peptide and the membrane. Thus the polylysine peptides are expected to have weaker membrane binding than the TAT peptide under the conditions of the two studies. The sensitivity of membrane binding to salt concentration is well-known and is exemplified by the fact that the free energies of polylysine binding decreased from -1.5 to -7 kcal/mol from 500 to 50 mM salt (49). The polylysine binding study also used lipid monolayers, where the lack of a distal membrane surface, with its concomitant anionic lipid headgroups, may weaken the propensity of the polylysines to insert into the membrane. In addition to these experimental differences, there is also a real difference in the affinity of Arg-rich and Lys-rich cationic peptides for the membrane interior. It is well-known that Lys substitution for Arg in cell-penetrating

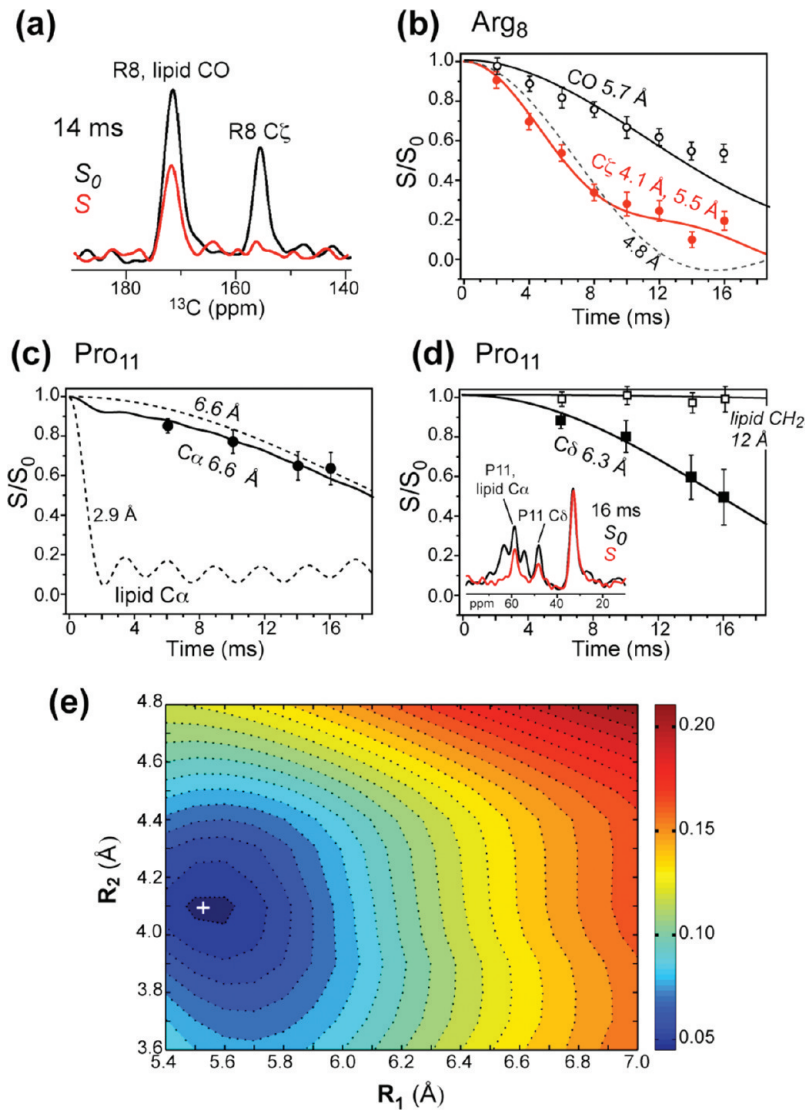


FIGURE 9:  $^{13}\text{C}$ - $^{31}\text{P}$  REDOR data of DMPC/DMPG-bound TAT at 230 K. (a) Representative REDOR control ( $S_0$ ) and dephased ( $S$ ) spectra. (b) REDOR data and simulation for Arg<sub>8</sub> CO and C $\zeta$ . The C $\zeta$  data are best fit by a 1:1 ratio of 4.1 and 5.5 Å. (c) REDOR data and best fit for Pro<sub>11</sub> C $\alpha$ . The lipid C $\alpha$  contribution (7% of full intensity) was taken into account by a fixed distance of 2.9 Å. (d) REDOR data and best fit for Pro<sub>11</sub> C $\delta$ . (e) rmsd between the simulated and experimental REDOR curves of Arg<sub>8</sub> C $\zeta$  to obtain the best-fit distances for C $\zeta$  in (b).

peptides abolishes the membrane translocation ability (50, 51). An increasing number of recent studies of CPPs and antimicrobial peptides suggested that the structural basis for this difference may lie in the ability of guanidinium to form hydrogen bond-stabilized bidentate complexes with lipid phosphates (12, 29, 40, 52), which cannot be achieved by the mobile amine of the Lys side chains.

Taken together, the interfacial location of the Arg-rich TAT in the lipid bilayer correlates well with the membrane translocation ability of the peptide and can be attributed to the strong electrostatic attraction between TAT and the anionic lipid membranes as well as hydrogen bond stabilization of the Arg residues by the lipid phosphates and water.

**TAT Perturbation of Lipid Membranes.**  $^{31}\text{P}$  NMR spectra of both neutral and anionic lipid membranes in the presence of TAT showed little isotropic disorder. The observation is reproduced in both aligned membranes and unoriented vesicle samples (Figure 5). This finding suggests that TAT binding does not significantly perturb the lamellar structure of the lipid bilayer. Interestingly, a detailed  $^{31}\text{P}$  NMR characterization of TAT binding as a function of membrane composition showed that the isotropic

disorder is a sensitive function of the acyl chain saturation and temperature (53). Low-melting lipids such as DLPC and POPC did not exhibit membrane disruption by TAT, while high-melting DMPC and DPPC bilayers were. Moreover, the nonlamellar disorder was only present in zwitterionic bilayers and not in anionic bilayers. The present use of unsaturated lipids in all three membrane series for the oriented  $^{31}\text{P}$  NMR experiments thus precluded the observation of any potential isotropic features. Our depth and conformational experiments were conducted in negatively charged lipid membranes, thus similarly precluding the observation of membrane disorder. When we applied two cycles of heating and cooling to the TAT-containing DMPC:DMPG (8:7) membrane sample, we did not observe an isotropic peak (Supporting Information Figure S2), which confirmed the lack of significant membrane disorder induced by thermal history.

Interestingly, an MD simulation of HIV TAT in a neutral DOPC bilayer as a function of peptide:lipid molar ratios found transient pores at high peptide concentrations (42). Based on these simulations, Herce and Garcia proposed that the mechanism of translocation involves membrane thinning, reorientation of the lipids near the peptide, and attraction of TAT to lipid headgroups on

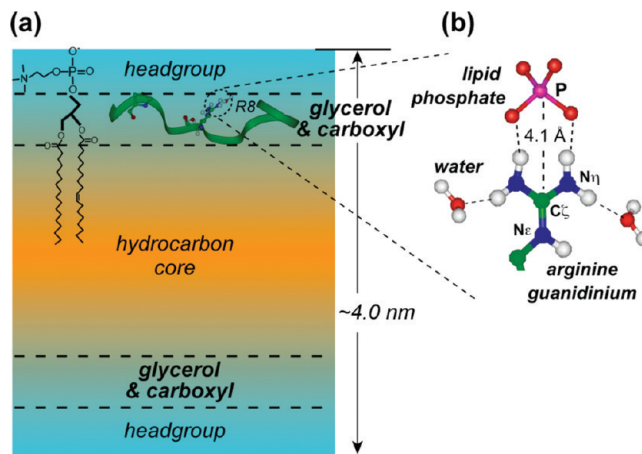


FIGURE 10: Model of TAT structure and dynamics in DMPC/DMPG bilayers. The random coil peptide is inserted into the bilayer at the glycerol backbone region, outside the hydrophobic core, and is stabilized by intermolecular hydrogen bonds with lipid phosphates and water. The glycerol region has intermediate dielectric constant and accommodates TAT through the polar phosphate and carboxyl groups, which can act as hydrogen bond acceptors for the guanidinium.

the distal (far) side of the membrane. The  $^{13}\text{C}$ - $^{31}\text{P}$  distances measured here support the latter two proposals. However, the lack of isotropic  $^{31}\text{P}$  signals indicates the absence of long-lasting pores, although our data, which describe the equilibrium state of the peptide, do not rule out the existence of transient pores during translocation. One possibility is that the Arg-phosphate salt bridge interaction may slow down the fast lipid lateral diffusion necessary for observing an isotropic signal, so that membrane defects may be present but undetectable in the  $^{31}\text{P}$  NMR spectra. However, we do not think this scenario is likely, because the salt bridge interaction is too weak (with a guanidinium  $N\eta$  order parameter of 0.30) to retard the lipid diffusion. Moreover, similar Arg-phosphate salt bridge interactions were observed in antimicrobial peptides such as PG-1 (29), which caused pronounced  $^{31}\text{P}$  isotropic features (39, 54).

**Random Coil Conformation of TAT in Lipid Bilayers.** The temperature-independent random coil chemical shifts of TAT and the temperature-dependent line width changes provide a rare example of a truly dynamic random coil peptide in lipid membranes. The 2D INADEQUATE spectra at low temperatures (Figure 1) exhibited fine structures for some side chain peaks. However, the chemical shift differences between the multiple peaks of each site are small compared to the line widths; thus they do not change the qualitative conclusion that the TAT adopts a random coil conformation in the lipid membrane.

While TAT is known to be unstructured in solution (30), the finding that it remains a random coil in the lipid bilayer is still surprising, since it is generally believed that unstructured peptides in solution acquire hydrogen-bonded canonical conformations upon membrane binding to reduce the number of polar N-H and C=O groups exposed to the membrane (45). In light of the lipid-peptide interaction data here, we propose that TAT remains random coil by substituting intramolecular hydrogen bonds by intermolecular ones with the lipid phosphates and water and by residing in the membrane-water interface, which has a higher dielectric constant than the hydrocarbon region of the bilayer. The intermolecular Arg-phosphate interaction is not only revealed by the short guanidinium-phosphate distance but also by the fact that the guanidinium exhibits higher order parameters than the rest of the Arg side chain. This lipid anchoring effect dovetails

a recent solution NMR and MD simulation study of Arg side chains in ribonuclease H, where the dynamics of the guanidinium  $N\epsilon$  was found to be primarily governed by salt bridges and was decoupled from the dynamics of the rest of the aliphatic side chain (55).

The random coil backbone should facilitate TAT interaction with multiple lipid headgroups, whose positions in the fluid bilayer are highly disordered. The completeness of the Arg<sub>8</sub>  $C\zeta$ - $^{31}\text{P}$  REDOR dephasing (Figure 9) confirms that all peptide molecules, instead of just a fraction, experience guanidinium-phosphate interactions. Finally, a random coil backbone reduces the hydrophobic surface of TAT and prevents any defined polar/apolar separation. In this way, the peptide may rapidly cross the bilayer instead of being retained permanently in the membrane, as is the case for amphipathic antimicrobial peptides. Since the intermolecular lipid-TAT and water-TAT hydrogen bonds can be formed for any phospholipid membranes, TAT is expected to adopt similar random coil structures in any anionic membranes. This prediction is supported by the fact that the same random coil chemical shifts were found in both DMPC/DMPG membranes and POPE/POPG membranes, even though PE membranes appear to permit more efficient translocation of TAT than PC membranes (52).

## CONCLUSION

In summary, using solid-state NMR we found that HIV TAT-(48–60) adopts a random coil conformation and inserts into the glycerol backbone region of the membrane–water interface in anionic lipid bilayers. This structure is thermodynamically stabilized by electrostatic attraction with the anionic lipids, guanidinium-phosphate salt bridges, and guanidinium–water hydrogen bonding. The highly dynamic TAT does not cause permanent damages to the membrane integrity but may cause transient defects, as suggested by short guanidinium–phosphate distances. These results suggest that TAT translocation is an extremely rapid phenomenon that relies on transient interactions of the Arg side chains with lipid phosphates of the distal leaflet. The equilibrium structure observed by solid-state NMR, showing the peptide lying at the membrane–water interface of both leaflets, is the structure after translocation. Catching the peptide “in action”, during translocation, may require independent experiments of the kind that has been used to probe transient macromolecular interactions and structural changes in solution (56, 57). We postulate that the role of the random coil conformation is to prevent the peptide from permanently residing in the hydrocarbon core of the lipid bilayer through hydrophobic interactions. The dynamic nature of TAT, together with the previously reported dynamic turn-rich conformation of penetratin, suggests that the Arg-rich CPPs differ from the Arg-rich amphipathic AMPs mainly by the presence or absence of intramolecular hydrogen-bonded conformations (14).

## SUPPORTING INFORMATION AVAILABLE

Static  $^{31}\text{P}$  spectra of TAT-containing unoriented DMPC/DMPG membranes under two heating and cooling cycles and a summary table of the solid-state NMR experiments. This material is available free of charge via the Internet at <http://pubs.acs.org>.

## REFERENCES

- Torchilin, V. P. (2008) Tat peptide-mediated intracellular delivery of pharmaceutical nanocarriers. *Adv. Drug Delivery Rev.* 60, 548–558.

2. Brooks, H., Lebleu, B., and Vives, E. (2005) Tat peptide-mediated cellular delivery: back to basics. *Adv. Drug Delivery Rev.* 57, 559–577.
3. Inomata, K., Ohno, A., Tochio, H., Isogai, S., Tenno, T., Nakase, I., Takeuchi, T., Futaki, S., Ito, Y., Hiroaki, H., and Shirakawa, M. (2009) High-resolution multi-dimensional NMR spectroscopy of proteins in human cells. *Nature* 485, 106–110.
4. Vives, E., Brodin, P., and Lebleu, B. (1997) A Truncated HIV-1 Tat protein basic domain rapidly translocates through the plasma membrane and accumulates in the cell nucleus. *J. Biol. Chem.* 272, 16010–16017.
5. Derossi, D., Joliot, A. H., Chassaing, G., and Prochiantz, A. (1994) The third helix of the *Antennapedia* homeodomain translocates through biological membranes. *J. Biol. Chem.* 269, 10444–10450.
6. Rothbard, J. B., Jessop, T. C., Lewis, R. S., Murray, B. A., and Wender, P. A. (2004) Role of membrane potential and hydrogen bonding in the mechanism of translocation of guanidinium-rich peptides into cells. *J. Am. Chem. Soc.* 126, 9506–9507.
7. Rothbard, J. B., Jessop, T. C., and Wender, P. A. (2005) Adaptive translocation: the role of hydrogen bonding and membrane potential in the uptake of guanidinium-rich transporters into cells. *Adv. Drug Delivery Rev.* 57, 495–504.
8. Fischer, R., Fotin-Mleczek, M., Hufnagel, H., and Brock, R. (2005) Break on through to the other side: biophysics and cell biology shed light on cell-penetrating peptides. *ChemBioChem* 6, 2126–2142.
9. Hessa, T., Kim, H., Bihlmaier, K., Lundin, C., Boekel, J., Andersson, H., Nilsson, I., White, S. H., and von Heijne, G. (2005) Recognition of transmembrane helices by the endoplasmic reticulum translocon. *Nature* 433, 377–381.
10. Derossi, D., Calvet, S., Trembleau, A., Brunissen, A., Chassaing, G., and Prochiantz, A. (1996) Cell internalization of the third helix of the *Antennapedia* homeodomain is receptor-independent. *J. Biol. Chem.* 271, 18188–18193.
11. Binder, H., and Lindblom, G. (2003) Charge-dependent translocation of the Trojan peptide penetratin across lipid membranes. *Biophys. J.* 85, 982–995.
12. Su, Y., Mani, R., and Hong, M. (2008) Asymmetric insertion of membrane proteins in lipid bilayers by solid-state NMR paramagnetic relaxation enhancement: a cell-penetrating peptide example. *J. Am. Chem. Soc.* 130, 8856–8864.
13. Su, Y., Doherty, T., Waring, A. J., Ruchala, P., and Hong, M. (2009) Roles of arginine and lysine residues in the translocation of a cell-penetrating peptide from  $^{13}\text{C}$ ,  $^{31}\text{P}$ , and  $^{19}\text{F}$  solid-state NMR. *Biochemistry* 48, 4587–4595.
14. Su, Y., Mani, R., Doherty, T., Waring, A. J., and Hong, M. (2008) Reversible sheet-turn conformational change of a cell-penetrating peptide in lipid bilayers studied by solid-state NMR. *J. Mol. Biol.* 381, 1133–1144.
15. Frankel, A. D., and Pabo, C. O. (1988) Cellular uptake of the Tat protein from human immunodeficiency virus. *Cell* 55, 1189–1193.
16. Fawell, S., Seery, J., Daikh, Y., Moore, C., Chen, L. L., Pepinsky, B., and Barsoum, J. (1994) Tat-mediated delivery of heterologous proteins into cells. *Proc. Natl. Acad. Sci. U.S.A.* 91, 664–668.
17. Eguchi, A., Akuta, T., Okuyama, H., Senda, T., Yokoi, H., Inokuchi, H., Fujita, S., Hayakawa, T., Takeda, K., Hasegawa, M., and Nakanishi, M. (2001) Protein transduction domain of HIV-1 Tat protein promotes efficient delivery of DNA into mammalian cells. *J. Biol. Chem.* 276, 26204–26210.
18. Gennis, R. B. (1989) Biomembranes: Molecular Structure and Function, Springer, New York.
19. Hallock, K. J., Henzler Wildman, K., Lee, D. K., and Ramamoorthy, A. (2002) An innovative procedure using a sublimable solid to align lipid bilayers for solid-state NMR studies. *Biophys. J.* 82, 2499–2503.
20. Hohwy, M., Rienstra, C. M., Jaroniec, C. P., and Griffin, R. G. (1999) Fivefold symmetric homonuclear dipolar recoupling in rotating solids: application to double-quantum spectroscopy. *J. Chem. Phys.* 110, 7983–7992.
21. Takegoshi, K., Nakamura, S., and Terao, T. (2001) C-13-H-1 dipolar-assisted rotational resonance in magic-angle spinning NMR. *Chem. Phys. Lett.* 344, 631–637.
22. Hong, M. (1999) Solid-state dipolar INADEQUATE NMR spectroscopy with a large double-quantum spectral width. *J. Magn. Reson.* 136, 86–91.
23. Huster, D., Yao, X. L., and Hong, M. (2002) Membrane protein topology probed by  $^1\text{H}$  spin diffusion from lipids using solid-state NMR spectroscopy. *J. Am. Chem. Soc.* 124, 874–883.
24. Hong, M., Gross, J. D., Rienstra, C. M., Griffin, R. G., Kumashiro, K. K., and Schmidt-Rohr, K. (1997) Coupling amplification in 2D MAS NMR and its application to torsion angle determination in peptides. *J. Magn. Reson.* 129, 85–92.
25. Munowitz, M. G., Griffin, R. G., Bodenhausen, G., and Huang, T. H. (1981) Two-dimensional rotational spin-echo nuclear magnetic resonance in solids: correlation of chemical shift and dipolar interactions. *J. Am. Chem. Soc.* 103, 2529–2533.
26. Rhim, W. K., Elleman, D. D., and Vaughan, R. W. (1973) Analysis of multiple pulse NMR in solids. *J. Chem. Phys.* 59, 3740–3749.
27. Huster, D., Xiao, L. S., and Hong, M. (2001) Solid-state NMR investigation of the dynamics of colicin Ia channel-forming domain. *Biochemistry* 40, 7662–7674.
28. Jaroniec, C. P., Toung, B. A., Herzfeld, J., and Griffin, R. G. (2001) Frequency selective heteronuclear dipolar recoupling in rotating solids: accurate  $(^{13}\text{C})-(^{15}\text{N})$  distance measurements in uniformly  $(^{13}\text{C})-(^{15}\text{N})$ -labeled peptides. *J. Am. Chem. Soc.* 123, 3507–3519.
29. Tang, M., Waring, A. J., and Hong, M. (2007) Phosphate-mediated arginine insertion into lipid membranes and pore formation by a cationic membrane peptide from solid-state NMR. *J. Am. Chem. Soc.* 129, 11438–11446.
30. Shojania, S., and O'Neil, J. D. (2006) HIV-1 Tat is a natively unfolded protein: the solution conformation and dynamics of reduced HIV-1 Tat(1–72) by NMR spectroscopy. *J. Biol. Chem.* 281, 8347–8356.
31. Wang, Y., and Jardetzky, O. (2002) Probability-based protein secondary structure identification using combined NMR chemical-shift data. *Protein Sci.* 11, 852–861.
32. Ziegler, A., LiBlatter, X., Seelig, A., and Seelig, J. (2003) Protein transduction domains of HIV-1 and SIV TAT interact with charged lipid vesicles. Binding mechanism and thermodynamic analysis. *Biochemistry* 42, 9185–9194.
33. Cady, S. D., and Hong, M. (2009) Effects of amantadine binding on the dynamics of bilayer-bound influenza A M2 transmembrane peptide studied by NMR relaxation. *J. Biomol. NMR* 45, 185–196.
34. Hong, M., Schmidt-Rohr, K., and Pines, A. (1995) Measurement of signs and magnitudes of C-H dipolar couplings in lecithin. *J. Am. Chem. Soc.* 117, 3310–3311.
35. Lesage, A., Emsley, L., Penin, F., and Böckmann, A. (2006) Investigation of dipolar-mediated water-protein interactions in microcrystalline Crh by solid-state NMR spectroscopy. *J. Am. Chem. Soc.* 128, 8246–8255.
36. Lesage, A., Gardiennet, C., Loquet, A., Verel, R., Pintacuda, G., Emsley, L., Meier, B. H., and Böckmann, A. (2008) Polarization transfer over the water-protein interface in solids. *Angew. Chem., Int. Ed.* 47, 5851–5854.
37. Doherty, T., and Hong, M. (2009) 2D  $^1\text{H}-^{31}\text{P}$  solid-state NMR studies of the dependence of inter-bilayer water dynamics on lipid headgroup structure and membrane peptides. *J. Magn. Reson.* 196, 39–47.
38. Mani, R., Cady, S. D., Tang, M., Waring, A. J., Lehrer, R. I., and Hong, M. (2006) Membrane-dependent oligomeric structure and pore formation of a beta-hairpin antimicrobial peptide in lipid bilayers from solid-state NMR. *Proc. Natl. Acad. Sci. U.S.A.* 103, 16242–16247.
39. Tang, M., and Hong, M. (2009) Structure and mechanism of beta-hairpin antimicrobial peptides in lipid bilayers from solid-state NMR spectroscopy. *Mol. Biosys.* 5, 317–322.
40. Tang, M., Waring, A. J., Lehrer, R., and Hong, M. (2008) Effects of guanidinium-phosphate hydrogen bonding on the membrane-bound structure and activity of an arginine-rich membrane peptide from solid-state NMR spectroscopy. *Angew. Chem., Int. Ed.* 47, 3202–3205.
41. Lensink, M. F., Christiaens, B., Vandekerckhove, J., Prochiantz, A., and Rosseneu, M. (2005) Penetratin-membrane association: W48/R52/W56 shield the peptide from the aqueous phase. *Biophys. J.* 88, 939–952.
42. Herce, H. D., and Garcia, A. E. (2007) Molecular dynamics simulations suggest a mechanism for translocation of the HIV-1 TAT peptide across lipid membranes. *Proc. Natl. Acad. Sci. U.S.A.* 104, 20805–20810.
43. Wimley, W. C., and White, S. H. (1996) Experimentally determined hydrophobicity scale for proteins at membrane interfaces. *Nat. Struct. Biol.* 3, 842–848.
44. Goncalves, E., Kitas, E., and Seelig, J. (2005) Binding of oligoarginine to membrane lipids and heparan sulfate: structural and thermodynamic characterization of a cell-penetrating peptide. *Biochemistry* 44, 2692–2702.
45. White, S. H., and Wimley, W. C. (1999) Membrane protein folding and stability: physical principles. *Annu. Rev. Biophys. Biomol. Struct.* 28, 319–365.
46. Freites, J. A., Tobias, D. J., von Heijne, G., and White, S. H. (2005) Interface connections of a transmembrane voltage sensor. *Proc. Natl. Acad. Sci. U.S.A.* 102, 15059–15064.
47. Li, L., Vorobyov, I., and Allen, T. W. (2008) Potential of mean force and pKa profile calculation for a lipid membrane-exposed arginine side chain. *J. Phys. Chem. B* 112, 9574–9587.

48. MacCallum, J. L., Bennett, W. F., and Tielemans, D. P. (2008) Distribution of amino acids in a lipid bilayer from computer simulations. *Biophys. J.* **94**, 3393–3404.
49. Ben-Tal, N., Honig, B., Peitzsch, R. M., Denisov, G., and McLaughlin, S. (1996) Binding of small basic peptides to membranes containing acidic lipids: theoretical models and experimental results. *Biophys. J.* **71**, 561–575.
50. Wender, P. A., Mitchell, D. J., Pattabiraman, K., Pelkey, E. T., Steinman, L., and Rothbard, J. B. (2000) The design, synthesis, and evaluation of molecules that enable or enhance cellular uptake: peptoid molecular transporters. *Proc. Natl. Acad. Sci. U.S.A.* **97**, 13003–13008.
51. Mitchell, D. J., Kim, D. T., Steinman, L., Fathman, C. G., and Rothbard, J. B. (2000) Polyarginine enters cells more efficiently than other polycationic homopolymers. *J. Pept. Res.* **56**, 318–325.
52. Mishra, A., Gordon, V. D., Yang, L., Coridan, R., and Wong, G. C. L. (2008) HIV TAT forms pores in membranes by inducing saddle-splay curvature: potential role of bidentate hydrogen bonding. *Angew. Chem., Int. Ed. Engl.* **47**, 2986–2989.
53. Afonin, S., Frey, A., Bayerl, S., Fischer, D., Wadhwan, P., Weinkauf, S., and Ulrich, A. S. (2006) The cell-penetrating peptide TAT(48–60) induces a non-lamellar phase in DMPC membranes. *ChemPhysChem* **7**, 2134–2142.
54. Mani, R., Buffy, J. J., Waring, A. J., Lehrer, R. I., and Hong, M. (2004) Solid-state NMR investigation of the selective disruption of lipid membranes by protegrin-1. *Biochemistry* **43**, 13839–13848.
55. Trbovic, N., Cho, J. H., Abel, R., Friesner, R. A., Rance, M., and Palmer, A. G. r. (2009) Protein side-chain dynamics and residual conformational entropy. *J. Am. Chem. Soc.* **131**, 615–622.
56. Iwahara, J., and Clore, G. M. (2006) Detecting transient intermediates in macromolecular binding by paramagnetic NMR. *Nature* **440**, 1227–1230.
57. Lee, M. K., Gal, M., Frydman, L., and Varani, G. (2010) Real-time multidimensional NMR follows RNA folding with second resolution. *Proc. Natl. Acad. Sci. U.S.A.* **107**, 9192–9197.
58. Luca, S., Filippov, D. V., van Boom, J. H., Oschkinat, H., de Groot, H. J., and Baldus, M. (2001) Secondary chemical shifts in immobilized peptides and proteins: a qualitative basis for structure refinement under magic angle spinning. *J. Biomol. NMR* **20**, 325–331.